Correlation between ion-exchange properties and swelling/shrinking processes in hexasulfonated calix[6]arene doped polypyrrole films: ac-electrogravimetry and electrochemical atomic force microscopy investigations

Loan To Thi Kim, Claude Gabrielli, Alain Pailleret, Hubert Perrot

Correlation between ion-exchange properties and swelling/shrinking processes in hexasulfonated calix[6]arene doped polypyrrole films : *ac*-electrogravimetry and electrochemical atomic force microscopy investigations

L.T.T. Kim[1,2], C. Gabrielli[1,2], A. Pailleret[1,2] and H. Perrot[1,2]

[1]CNRS, UPR 15, LISE, F-75005, Paris, France.
[2]UPMC Univ. Paris 06, UPR 15, LISE, F-75005, Paris, France.
Tel: + 33 1 44 27 72 16 ; Fax: + 33 1 44 27 40 74

Abstract

Electrogenerated polypyrrole films doped with hexasulfonated calix[6]arenes were subjected to *ac*-electrogravimetry and electrochemical atomic force microscopy (EC-AFM) studies in aqueous potassium nitrate solutions. The former technique reveals that these films are mainly cation exchangers although solvent molecules (H_2O) and anions (NO_3^-) are also exchanged, in much lower amounts, in the course of the doping/undoping process. Unexpectedly, within the potential range encompassing this process, K^+ cations were found to be exchanged for more cathodic potentials whereas H_3O^+ are exchanged for more anodic potentials. EC-AFM investigations revealed substantial shrinking and swelling during the oxidation (doping) and reduction (undoping) processes respectively. An obvious correlation can easily be built between these observations: the oxidation of the polymer films provokes an expulsion of the cations, as expected from cation exchanger polymer films, and therefore a decrease of the volume (and thickness) of these films whereas their reduction causes an insertion of cations and an increase of their volume (and thickness). This electromechanical mechanism is amplified by the simultaneous exchange of free water molecules. Suggestions based on these observations, on structural characteristics of polypyrrole films, and on complexation ability of hexasulfonated calix[6]arenes incorporated in the films are discussed to explain i) the change of the identity of the exchanged cations as a function of the potential, ii) the exchange of free water molecules and, iii) the exchange of small amounts of nitrate ions.

1. Introduction

Calixarenes are metacyclophanes produced from the condensation of phenol with formaldehyde [1,2]. As they are poorly soluble in water, the necessity of appending ionic functional groups, such as carboxylic acid (-COOH) or sulfonic acid ($-SO_3H$) groups at the

para-position of the phenolic units has been reported in literature (see [3,4] and Chapter 24 in [1]). Sulfonated calix[n]arenes are consequently versatile water–soluble binding agents able to bind with a significant selectivity a large set of interesting species, whether these latter are molecular or mono-atomic, ionic or neutral, and organic, inorganic or biological [5]. In the case of hexasulfonated calix[6]arenes (C6S) employed in this contribution, let us cite as possible targeted analytes in a non-exhaustive list, UO_2^{2+} and some transition metal (Ni^{2+}, Zn^{2+}, Cu^{2+}, Fe^{3+}) [6,7] and lanthanide [8] cations, ferrocene and cobaltocenium derivatives [9-12], quaternary ammonium cations [13], cationic surfactants [14,15], neutral molecules [16], as well as proteins (such as Bovine Serum Albumine (BSA)), amino-acids, oligo-peptides, drugs, and other small bioactive molecules [17-18] and even iron oxide nanoparticules [19].

Among the various applications of these versatile complexation behaviours, the elaboration of calixarene based electrochemical sensors has been thoroughly investigated although it required the exploration of strategies allowing the immobilisation of sulfonated calixarenes on classical working electrode surfaces. One way to achieve this goal consists in using these ionic calixarenes as doping anions in electronically conducting polymer matrices (films or colloids) such as polypyrrole [20-22], poly-(ethylene-dioxy-thiophene) (PEDOT) [23] or polyaniline [24]. The elaboration of electrochemical sensors based on this strategy will succeed only on condition that the calixarene based dopants conserve the binding character and the selectivity they display in solution once they are incorporated in the polymer matrix, which was shown to be achieved for C6S doped polypyrrole films with a targeted analyte such as uranyle cations [22]. Interestingly, the success of this strategy will also rely on the ion exchange properties of the resulting C6S doped conducting polymer films, which in turn depend, for a part, on the structural characteristics of these films possibly at the nanometric or molecular scale. Let us notice here that information on the structural characterisation is poor in literature in the case of electrodeposited electronically conducting polymers (ECP) films.

The purpose of this contribution was first to develop a deep understanding of ion (and potentially solvent) exchanges taking place in electrodeposited C6S doped polypyrrole (PPy) films during electrochemically controlled doping/undoping using *ac*-electrogravimetry experiments based on a well-established procedure.

Our second intention was to identify the electromechanical (swelling/shrinking) behaviour resulting presumably from these ions and solvent exchanges in our PPy/C6S films. A few research groups have indeed developed strategies allowing the accurate *in-situ* measurement of these volume (and topographical) changes under electrochemical control of the doping state of the polymer film either at locale or global scale [25-34]. In this

contribution, we used electrochemical atomic force microscopy (also referred to as EC-AFM), i.e. AFM in an electrolytic solution allowing an electrochemical conditioning of the substrate (C6S doped PPy films in this contribution).

2. Experimental part

2.1. Electrochemical deposition of PPy/C6S thin films

Hexasulfonated calix[6]arene doped polypyrrole (PPy/C6S) thin films were electrochemically deposited from aqueous solutions containing the pyrrole monomer (0,1 M) and hexasulfonated calix[6]arene (C6S, 1,66 10^{-3} M, see its structure on scheme 1). Such electrolytic solution was always prepared immediately prior the electropolymerisation was launched so as to avoid the formation of insulating polypyrrole particles via an autopolymerisation mechanism reported in literature [35]. The six sulfonic acid groups all possess a same and very low pKa value which was suggested to be below 1, as reported in [36]. On the other hand, the acidic power of the six phenolic protons (OH groups) is measured by different pKa values revealing intramolecular hydrogen bonds resulting from the removal of one or several of these phenolic protons. As a poly-acid, C6S was shown to possess only two ionisable OH groups in the pH range 2,5-7 (pKa_1 = 3,37-3,45 and pKa_2 = 4,76-5,02) whereas the remaining four phenol groups are only weakly acidic (pKa_3 > 11) [36-38]. As a consequence, the pH of our electrolytic solutions used for the electrodeposition step is expected to be 2, which is largely above the pKa values of the sulfonic acid groups and below that of the phenolic protons. C6S is thus expected to be hexa-anionic in this electrolytic solution. In spite of the low ionic strength of the resulting electrodeposition solution, no other background salt was added in the electrodeposition solution so as to make sure that the produced PPy films were doped with hexasulfonated calixarenes only, and display therefore ion exchange properties resulting only from the incorporation of those large anions during the electrodeposition step. The electrochemical technique used for the electrodeposition of these films was cyclic voltammetry. The potential range chosen for this electrodeposition step extends from -1 V to 0,4 V vs an aqueous K_2SO_4 saturated mercurous sulphate (SSE) reference electrode so as to avoid the electrochemical oxidation (and subsequent degradation) of the hexasulfonated calix[6]arene anions as reported in literature [39-41]. PPy films dedicated to EC-AFM investigations were electrodeposited on a working electrode made of a thin layer of platinum (thickness: $\approx$ 60 nm, RMS : $\approx$ 2,5 nm, area: 0,126 cm^2) deposited on

mica through a mask using the sputtering technique. Those dedicated to *ac*-electrogravimetry (and cyclic electrogravimetry) investigations were electrogenerated on a quartz bearing a key shaped gold electrode on each of its two faces. A typical voltammogram corresponding to the electrodeposition of these films in these experimental conditions is shown on Figure 1. SEM-FEG imaging of the profile of the obtained film reveals a thickness close to 500 nm. This is only an estimation as it was measured in vacuum conditions required by SEM-FEG imaging. As a consequence, it is definitely not the thickness of a fully water-loaded and hydrated film.

2.2. *Ac*-electrogravimetry investigations

The experimental procedure and setup used to carry out the *ac*-electrogravimetry experiments have been reported elsewhere in previous publications of our group [42-45]. The quartz crystals used in the present investigations have a base frequency of 9 MHz.

2.3. EC-AFM measurements

EC-AFM experiments required a home made electrochemical cell in which the working electrode bearing the PPy film lies flat in the back of the cell whereas a platinum grid and a silver wire covered with an electrogenerated silver chloride film are used respectively as counter- and Ag/AgCl reference electrodes respectively. A SP300 potentiostat (Bio-Logic, Claix, France) is connected simultaneously to i) this electrochemical cell so as to apply various potential conditionings and to read the resulting current on the working electrode and ii) the AFM controller (Picoscan 2100, Agilent, USA) so as to allow this latter to read these two signals at the acquisition frequency of the data related to proper AFM imaging. This was also necessary so as to insure a perfect synchronization of the acquisition of height, potential and current data. AFM imaging was performed in-situ in a transfer electrolytic solution (0,1 M KNO_3 aqueous solution) in the contact mode on a 1 nm^2 area using triangular AFM cantilevers (PNP-TR, NanoWorld, Paris, France) characterised by a low spring constant ($k_N \approx$ 0,08 N m^{-1}). A 1 nm^2 scanned area was chosen as it is expected to be much smaller than the contact area between the tip and the polymer sample. This choice led in a first approximation to a situation where the tip can be considered immobile in the x-y plane of the sample, and behaves therefore as a profilometer measuring the variation of the thickness of the film (and not the thickness itself) regardless of the local roughness and roughness changes also expected to occur in our experimental conditions on the investigated samples. The scan rate of the

AFM tip was chosen in the range 0,5 to 2 Hz in order to provide an imaging duration longer than that required for the corresponding potential conditioning (consecutive cyclic voltammetry scans or consecutive potential steps for example) applied on the polymer film.

3. Results

3.1. Cyclic electrogravimetry

After transfer in a KNO_3 aqueous electrolytic solution, PPy/C6S films electrodeposited in the experimental conditions described above can be electrochemically and reversibly doped and undoped using cyclic voltammetry, as revealed respectively by the oxidation and reduction waves appearing on the resulting voltammogram (see Figure 2a). Cyclic voltamassograms obtained simultaneously from cyclic electrogravimetry experiments show that the oxidation/reduction of these films leads to substantial loss/gain of mass (see Figure 2b). By combining current and mass measurements, the atomic weight of the charged species, m_i, involved in the electrochemical process can be easily estimated by using the following equation : $m_i = F\dfrac{dm}{dq} = F\dfrac{dm}{dt} \times \dfrac{1}{i}$. Following the potential scan, the atomic weight determined for the exchanged species varies between 40 g mole^{-1} and 0 g mole^{-1} without reaching any stable values. It indicates certainly a mixed contribution of cations without excluding the participation of the solvent and/or the anions. This point underlines the limitation of the cyclic electrogravimetry technique where only one scan rate was used for a large exploration of the potential. Furthermore, the molar mass of the exchanged species was not constant over the whole potential range, as shown from Figure 2c. These mass variations were therefore not quantitatively exploited here as *ac*-electrogravimetry experiments reported hereafter are much more powerful to establish a comprehensive understanding of ions and solvent exchanges taking place during doping/undoping processes. Both cyclic voltammograms and cyclic voltamassograms were found to be stable for a film stored in an aqueous KNO_3 solution during three days (see Figure 2a-b).
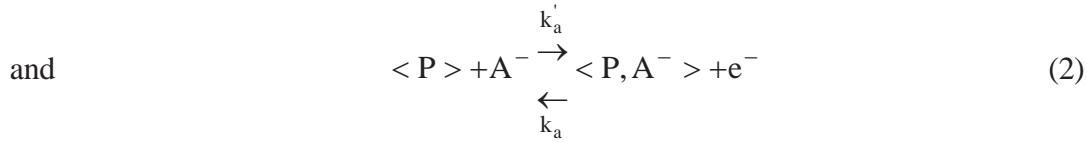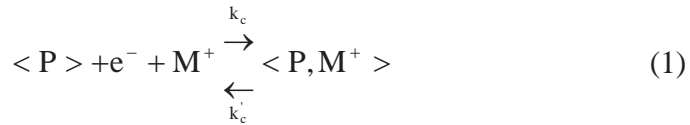
3.2. *Ac*-electrogravimetry

3.2.1. Theory

In this approach, where the PPy/C6S film is coated on the gold electrode of the quartz crystal, charge transfer at the electrode/film interface, mass transport in the solution and in the film are considered to be fast compared to the charge transfer at the film/solution interface,

which is considered as the rate limiting step. This hypothesis is justified for thin films where, in addition, the quartz crystal is working in the gravimetric mode (i.e. no viscoelastic distortion occurs). For the thin films used in this work, EIS spectra did not show any 45° slope, which demonstrates that diffusion is not a limiting step [46]. Here, only one cation (solvated or not), one anion, and one free solvent, i.e. solvent not involved in the solvation shell of an ion, are considered, for monocharged ions, to be exchanged with the solution to compensate the charge displacement occurring during oxidation or reduction of the electroactive film to reach electroneutrality in the film.

The doping mechanism of an electroactive film can be described simply by:

$$<P> + e^- + M^+ \underset{k_c'}{\overset{k_c}{\rightleftarrows}} <P, M^+> \tag{1}$$

and

$$<P> + A^- \underset{k_a}{\overset{k_a'}{\rightleftarrows}} <P, A^-> + e^- \tag{2}$$

where <P> is the host electroactive film, <P,M$^+$>, et <P,A$^-$> the inserted cation and anion in the film matrix. Therefore, the net instantaneous molar flux of species i (c, a or s) is J_i (mol cm^{-2} s^{-1}) and it can be obtained by applying the classical kinetic laws for heterogenous reactions. The flux of the species C_i is equal for each ions to:

$$J_i(d) = -d_f \frac{dC_i}{dt} = k_i (C_i - C_{i_{min}}) - k'_i (C_{i_{max}} - C_i) C_{i_{sol}} \tag{3}$$

where d_f is the thickness of the film and $\frac{dC_i}{dt} > 0$ for inserted species, $C_{i_{max}}$, is the maximum concentration of the sites available for insertion, $C_{i_{min}}$ is the minimum concentration of the sites occupied by the species in the host film, $C_{i_{sol}}$ is the concentration of species i in the solution and k_i and k'_i are the kinetic rate constants of transfers, according to the classical Tafel laws $k_i = k_{i0} \, exp \, b_i \left(E - E_i^0 \right)$ and $k'_i = k'_{i0} \, exp \, b'_i \left(E - E_i^0 \right)$. Therefore, the fluxes of the involved species i (c, a or s), J_i, are positive for outgoing species:

$$J_i > 0 \qquad \text{for x} > 0 \qquad \text{i = a, c, s} \tag{4}$$

- Concerning the solvent movement, the following solvation model is considered [47]

$$<P^+> + xS \underset{k_s'}{\overset{k_s}{\rightleftarrows}} <P^+, S> \tag{5}$$

where <P+,S> is the solvated oxidized site and x the number of solvent molecule per oxidized site.

$$\frac{dC_s}{dt} = k_i \left(C_{P^+} - C_s \right) C_{s_{sol}}^x - k_i'\, C_s \tag{6}$$

However, $C_{s_{sol}} = \text{cst}$ and $C_{P^+} = C_{s\,max}$

$$\frac{dC_s}{dt} = k_i \left(C_{s\,max} - C_s \right) - k_i' \left(C_s - C_{s\,min} \right) \tag{7}$$

Then, the kinetic equations for the ions have the same form than those of ions. In dynamic regime, when a small sine wave potential change, ΔE, is imposed across the metal/film/electrolyte interfaces, low amplitude sine wave concentrations, ΔC_i, and fluxes, ΔJ_i, are observed at the film/solution interface (x = d_f), such as:

$$\Delta J_i(d_f) = -j\omega d_f \Delta C_i(d_f) = K_i \Delta C_i(d_f) + G_i \Delta E \qquad \text{where} \qquad i = c, a, s \tag{8}$$

As from Eq. (3)

where $$G_i \;=\; b_i k_i (\, C_i \; - C_{i\,min}\;) - b_i' k_i' (\, C_{i\,max}\; -\; C_i\,) \tag{9}$$

and, $$K_i \;=\; k_i \;+\; k_i' C_{isol} \tag{10}$$

where $G_i < 0$ for inserting species and $G_i > 0$ for expelling species.

Then, according to equ. (8) :

$$\frac{\Delta C_i}{\Delta E}(\omega) = \frac{-G_i}{j\omega d_f + K_i} \tag{11}$$

Thus, the $\dfrac{\Delta C_i}{\Delta E}(\omega)$ allows the electrochemical impedance, $\dfrac{\Delta E}{\Delta I}(\omega)$, and the electrogravimetric transfer function, $\dfrac{\Delta m}{\Delta E}(\omega)$ to be calculated.

The charge variation Δq is related to the Faradaic current density change, $\Delta I_F = j\omega \Delta q$, and by using eq. (8) it comes:

$$\frac{1}{j\omega}\frac{\Delta I_F}{\Delta E}(\omega) = d_f \left[-\frac{\Delta C_c}{\Delta E}(\omega) + \frac{\Delta C_a}{\Delta E}(\omega) \right] \tag{12}$$

and
$$\frac{\Delta m}{\Delta E}(\omega) = d_f\left[m_C\frac{\Delta C_c}{\Delta E}(\omega) + m_a\frac{\Delta C_a}{\Delta E}(\omega) + m_s\frac{\Delta C_s}{\Delta E}(\omega)\right]$$
(13)

where m_c, m_a and m_s are the atomic masses of the cations, anions, and solvent respectively.

Therefore, the electrochemical impedance, $\frac{\Delta E}{\Delta I}(\omega)$, which is measured, is equal to:

$$\frac{\Delta E}{\Delta I}(\omega) = \frac{1}{j\omega C_{dl} + \frac{\Delta I_F}{\Delta E}(\omega)}$$
(14)

where C_{dl} is the double layer capacitance, the electrolyte resistance being neglected here.

By using equ. (12) one obtains:

$$\frac{\Delta E}{\Delta I}(\omega) = \frac{1}{j\omega C_{dl} + j\omega d_f\left[\dfrac{G_c}{j\omega d_f + K_c} - \dfrac{G_a}{j\omega d_f + K_a}\right]}$$
(15)

and
$$\frac{\Delta m}{\Delta E}(\omega) = -d_f\left(m_C\frac{G_c}{j\omega d_f + K_c} + m_a\frac{G_a}{j\omega d_f + K_a} + m_s\frac{G_s}{j\omega d_f + K_s}\right)$$
(16)

Of course, only the charged species, anions and cations, are implied in the electrochemical impedance, $\frac{\Delta E}{\Delta I}(\omega)$, whereas the electrogravimetric transfer function, $\frac{\Delta m}{\Delta E}(\omega)$, depends on both cations, anions, and solvent all together.

Another interesting quantity can be calculated to discriminate the influence of the various species:

The electric charge/potential transfer function, $\frac{\Delta q}{\Delta E}(\omega)$, according to equ. (12) :

$$\frac{\Delta q}{\Delta E}(\omega) = \frac{1}{j\omega}\frac{\Delta I_F}{\Delta E}(\omega)$$
(17)

$$= d_f\left[-\frac{\Delta C_c}{\Delta E}(\omega) + \frac{\Delta C_a}{\Delta E}(\omega)\right]$$
(18)

$$= d_f\left[\frac{G_c}{j\omega d_f + K_c} - \frac{G_a}{j\omega d_f + K_a}\right]$$
(19)

3.2.2. Experiments

Simultaneous measurements of the electrochemical impedance $\frac{\Delta E}{\Delta I}(\omega)$ and of the electrogravimetric transfer function $\frac{\Delta m}{\Delta E}(\omega)$ were performed by using a technique already described elsewhere [42-45]. Figure 3 shows examples of the quantities of interest at various potentials, $\frac{\Delta m}{\Delta E}(\omega)$, together with the $\frac{\Delta q}{\Delta E}(\omega)$ transfer function calculated from $\frac{\Delta E}{\Delta I}(\omega)$ and using Eq. (17). By fitting the experimental data with Eqs. (16) and (19), both the kinetic parameters K_i and G_i, and the atomic masses of the ions and solvent , m_i, involved in the charge compensation process were obtained. Figure 4a and b show the change of the K_i and G_i / K_i ratios with respect to the potential. Concerning the atomic masses, values of 62 g mol^{-1} and 18 g mol^{-1} were obtained for the anions and solvent, respectively, which shows that nitrate ions and naturally water are involved. However, for the positive charges, an apparent atomic mass which varies with the potential was obtained (Figure 5). This demonstrates that the positive charges exchanged are mainly potassium in the cathodic potential domain whereas it is the solvated proton (hydronium H_3O^+) in the anodic range. From these data, two types of quantities can be deduced. First, as from Eq. $\frac{\Delta C_i}{\Delta E}(0) = -\frac{G_i}{K_i}$, the change of the concentrations of the species in the film with respect to the potential $\Delta C_i(E)$ can be obtained by integrating the values of $\frac{G_i}{K_i}(E)$ from Fig. 4b with respect to the potential from -0,6 V to 0,2 V vs SCE. Figure 6 shows that it is mainly the cations which are involved in the charge compensation: a large quantity of cations are expelled when the potential increases. Concomitantly, as shown in [46], some free water is also expelled with the cations whereas nitrate ions are inserted in the film when the potential increases, but in relatively small quantity compared to the cations.

So, knowing the total concentration of cations, and the relative quantity of potassium and hydronium ions (Figure 5) the concentrations of these two cations released from the film are obtained with respect to the potential. Figure 6 shows that, starting in the cathodic potential range, potassium ions are first expelled. When the potential increases hydronium ions begin to be expelled and then for larger potentials they constitute the major part of the positive species exchanged up to the anodic potentials where they are practically the only ions expelled.

3.3. EC-AFM

The variation of thickness occurring in ECPs during doping/undoping processes can be measured with a nanometric resolution using EC-AFM. Advantageously, this methodology resulting from the coupling of in-situ AFM in the contact mode with an electrochemical technique applied on the investigated samples is yet more promising due to the wide choice of electrochemical techniques that can be selected (cyclic voltammetry or chronoamperometry for example). Figure 7 shows the dynamics of the thickness variation of a PPy/C6S film during a series of consecutive potential steps applied vs an Ag/AgCl reference electrode. This potential conditioning is made of a series of four consecutive potential steps (-0,3 V, -0,7 V, 0,4 V, -0,7 V) whose duration was 30 seconds (see thin line on Figure 7d). This series of potential steps was repeated five times. -0,7 V and 0,4 V are two potential values encompassing the doping/undoping process of the film whereas -0,3 V is a potential value corresponding to the transition of identity (K^+ instead of H_3O^+) observed for the exchanged cations. Figures 7a, 7b and 7c are EC-AFM images showing respectively the variation of height, potential (with its sign inverted) and current measured on the PPy/C6S film. Let us notice that the bottom half of these images is featureless because it corresponds to a time range that followed the end of the potential conditioning applied on the film. The top half of these three images all show horizontal stripes, indicating that there is a correlation (or anticorrelation) between the height (and therefore film thickness), potential and current. On the potential image, each stripe corresponds to a potential step and each color change between two consecutive stripes results from a transition between two consecutive potential steps. Similar features are observed on the height image, indicating that height follows variations similar with those undergone by the potential applied on the working electrode/sample. Even though current image also shows stripes, small color variations can be observed inside individual stripes. They represent slight current variations occurring during potential steps that are nevertheless very weak by comparison with those occurring during potential transitions. Due to the size of the scanned area (1 nm^2) and knowing that the potential and current are relative to the whole film, Figures 7a, 7b and 7c should rather be considered as images showing the variation of these three parameters (height, potential, current) as a function of time. A better representation of these variations is thus given by graphs plotted as a function of time, as shown on Figure 7d. The current variation i= f(t) was not plotted for the need of clarity. By comparing Figures 7a-b between them or by comparing the two curves plotted on Figure 7d, one can first conclude that there is an anticorrelation between the

thickness of the film and the potential, and thus between its thickness and its oxidation state. More precisely, the more the film is oxidised, the thinner it gets. Interestingly, the thickening dynamics almost reaches a steady state over the 30 sec duration of each of the potential steps from -0,3 V to -0,7 V whereas during the large oxidation step from 0,4 V to -0,7 V, the steady state is not reached over the same duration. The lowest and highest thicknesses were observed for the most oxidising (+0,4 V) and reducing potentials (-0,7 V) respectively. The maximum thickness increase observed after reduction of an oxidised film over a 30 sec duration is approximately 500 nm, which would correspond to a 100 % variation of the thickness measured for the dry film using SEM. This 100 % value is likely to be an overestimation as the thickness measured for this film (in its reduced state) using SEM-FEG is likely to be underestimated. Indeed, one can easily admit that such films will substantially thicken upon water uptake when transferred from primary vacuum to an electrolytic aqueous solution, regardless of the doping/undoping processes regulated by a potential perturbation. The fact that the -0,4 V potential value corresponding to the transition of the exchanged cations (from K^+ to H_3O^+) led to an intermediate thickness value indicates that the film keeps thickening as it goes from the oxidised state to the reduced state whatever the identity of the incorporated cations is (K^+ or H_3O^+). The thickness variations observed on Figure 7d appear to be fairly reversible over five consecutive scans, indicating a good stability for the electromechanical behaviour of this film. One must also notice from Fig. 7d that for a potential step from -0,7 V to 0,4 V, the thickness of the PPy film decreases during the expulsion of cations before it starts increasing again possibly due to the insertion of anions [46].

Figures 8a, 8b and 8c have the same meaning as Figures 7a, 7b and 7c although they correspond to another potential conditioning of the film. As figure 7d, Figures 8d-e show the variation of the applied potential and of the thickness (these data were simply split into two graphs so as to facilitate the reading of the curves). The potential conditioning consists in five consecutive cyclic voltammetry procedures including each five consecutive scans at three different scan rates. This therefore leads to a conditioning made of 15 consecutive potential scans carried out over the adequate potential range (-0,7 V to 0,4 V vs Ag/AgCl). In the chronological order, the scan rates were 200, 100 (see Fig. 8d) and 50 mV s^{-1} (see Fig. 8e). One can first notice that a reduction or an oxidation of the film following a linear potential scan produce respectively a linear increase (swelling) or a linear decrease (shrinking) of its thickness (see mainly Figure 8d-e). Moreover, these thickness variations seem to be constant and reversible in a first approximation and also independent from the scan rate. For a very slow scan rate such as 10 mV s^{-1} (Figure not shown), the variation of the thickness over a

potential ramp is lower and seems to follow a more complex law made of two variation regimes separated by a short inversion of the direction of variation (.i.e two increase regimes separated by a short decrease for example, see Figure 8f)). The potential at which this separation occurs seems to correspond to the potential range in which the transition of the identity of the exchanged cations was observed from ac-electrogravimetry.

By plotting the thickness variation as a function of the applied potential for five consecutive scans at a given potential scan rate, one can establish new graphes showing swelling/shrinking cycles over the potential range used for these experiments. As an example, Figures 9a and 9b show the resulting graphes for 100 and 20 mV s^{-1} scan rates respectively. By analogy with cyclic voltamperograms or cyclic voltamassograms that show respectively the variation of current (in amperes) and mass (in grams) as a function of the potential, Figures 9a and 9b show voltathicknograms as they show the variation of thickness (in nanometers) as a function of the applied potential. Both of them show again a swelling of the film upon reduction and its shrinking upon oxidation, as already pointed out from Figure 8a-f but moreover they show an hysteresis loop comparable to that observed on cyclic voltamassograms, indicating that swelling and shrinking processes do not follow the same electromechanical path.

4. Discussion

One can reasonably expect that electrodeposited films of electronically conducting polymers undergo a variation of their thickness (swelling/shrinking) as a consequence of the ion exchanges constituting the electrochemically driven doping/undoping processes. Let us emphasise that exchanges of either free or solvating water molecules may also be observed at the film/electrolytic solution interface, with or without a directional and/or quantitative correlation with the ion exchanges. The sum of these solvent and ion exchanges is likely to result in a volume change of the films, although this latter may well depend on other simultaneous phenomena. Indeed, volume (and thus thickness) variations may also be influenced by changes of conjugation lengths produced by changes of the oxidation state of the polymer chains, or modifications of relative orientations of monomer molecules in the polymer chains due to changes of the conformational flexibility inside these latter. A variation of the hydrophilic character of polymer chains as a function of their oxidation state may also alter significantly chemical interactions between them and their subsequent stacking. Unfortunately, the consequence of this list of parameters and phenomena producing

swelling/shrinking phases makes their extent hardly predictable. Obviously, one should also keep in mind that the identity of the solvent and background salts used during the electrodeposition step and during the electrochemical doping/dedoping processes will bring another contribution, yet often unpredictable, on these swelling/shrinking processes due to their role on the interactions between the chains and their packing. From the conclusions of our experimental results obtained with the ac-electrogravimetry technique, it appears that the insertion of the cations occurs first, followed by that, slower, of free water molecules, during the reduction step from -0,3 V to -0,7 V and from 0,4 V to -0,7 V vs Ag/AgCl. This fast redox process involving in parallel cation exchanges, slower as deduced from Figure 3b, is represented by the top reaction appearing on scheme 2 [48-50]. This insertion of cations is clearly correlated with a thickening of the film (see Figure 7d). This is also particularly well illustrated by the obvious similarities existing between the voltamassogramms and voltathicknogramms shown respectively on Figures 2b and 9a-b. All show hysteresis loops with the same orientation and the same clockwise rotation with the applied potential. Concerning the oxidation step from -0,7 V to 0,4 V and from -0,7 V to -0,3 V, where cations and water are expelled, the film thickness decreases. When the film shrinks, it can be assumed that the porosity of the film decreases as well. This can explain why hydronium ions, which are smaller [51], are substituted to potassium ions to be the relevant ions that compensate the electric charge when the potential increases [52].

On the other side, during the reduction step from -0,3 V to -0,7 V, the cations, mainly potassium, are rapidly exchanged, which allows a steady state to be reached with a relatively short time constant of a few tens of seconds. On the opposite, during the oxidation step from -0,7 V to 0,4 V, the cations, mainly potassium first and then mainly hydronium, are expelled in a first step, which leads to a fast decrease of the film thickness, but after some time an increase of this latter is observed. Two origins can be envisaged for this tendency, either some nitrate anions which are slower than cations and water, as shown from Figure 3b, but much heavier than hydronium ions, may be inserted in the film or this slow thickening of the film may be due to some reorganization, or relaxation, of the film.

The exchange of anions (nitrate ions) revealed by the ac-electrogravimetry experiments can hardly be understood straightforward and it is obvious that the top reaction reported on scheme 2 does not allow to explain it. The ability of hexasulfonated calix[6]arenes to bind potassium cations can provide a precious help for this purpose. The vertical reactions on the left and right hand sides of scheme 2 reflect the complexation/decomplexation of potassium cations respectively in the oxidised and reduced

forms of C6S doped polypyrrole films. Indeed, C6S may well bind, only weakly, potassium cations as i) the ionic radius of these latter allows them to fit in the cavity offered by C6S, and ii) para-sulfonated phenol units of sulfonated calixarenes are known to participate in cation-π interactions with alkaline metal cations [5]. In our polypyrrole films, potassium cations are exchanged in their unsolvated form (molar mass = 39 g mol^{-1}), which may substantially improve their affinity for complexation by C6S although this latter depends also on the availability of C6S anions for this role once they are trapped inside polypyrrole films. In spite of that, one can take as a reasonable hypothesis that complexation of unsolvated potassium cations by C6S indeed occurs in these films, whether PPy/C6S films are in the oxidised or reduced state. It must then be noticed that the reduced form of C6S doped PPy films (see the PPy/C6S form in the bottom right corner of scheme 2) includes two different forms of potassium cations, i.e. free potassium cations available for transfer at the film/electrolyte interface and potassium cations strongly bound in the cavity of sulfonated calix[6]arenes. As a consequence, soaking of our PPy/C6S films electrodeposited in the reduced form from acidic solutions in aqueous potassium nitrate solutions would lead to the complexation of potassium cations in the C6S cavities, and thus to the incorporation of nitrate ions simultaneously for the need of electroneutrality. The electrochemical oxidation of the films would lead to an excess of cationic charges in the films by comparison with the amount of anionic charges provided by the irreversibly trapped C6S anions. The respect of the electroneutrality of the film would then require the incorporation of nitrate anions from the transfer electrolytic solution. This mechanism and the bottom reaction in scheme 2 are indeed advantageous as they provide a convincing explanation for the exchange of cations (potassium or hydronium cations) and nitrate ions in opposite directions, identified from our *ac*-electrogravimetry observations.

5. Conclusion

Electrodeposited polypyrrole films doped with hexasulfonated calix[6]arenes (C6S) were investigated in potassium nitrate aqueous solutions using cyclic electrogravimetry, ac-electrogravimetry and electrochemical atomic force microscopy (EC-AFM). In the course of electrochemically driven doping/undoping processes, the two former techniques provided an accurate identification of ion and free solvent exchanges occurring in these films whereas the latter one allowed in-situ characterisation of swelling/shrinking processes.

The investigated films were found to be mainly cation exchangers, as a result of the irreversible incorporation of bulky C6S anions in the PPy matrix during the electrodeposition

step. The identity of these cations (K^+ or H_3O^+) depends on the potential inside the potential range encompassing the doping/undoping reactions. Free solvent (water) molecules are also exchanged simultaneously, in much lower amounts, in the same direction than cations. Nitrate anions were found to be exchanged, but in an opposite direction, as they penetrate inside the films upon oxidation and are expulsed out of it upon reduction. This minor anion exchanger character is possibly due to the complexation of potassium cations inside the trapped C6S cavities whether the polymeric matrix is in an oxidised or reduced state.

EC-AFM investigations were carried out by using the AFM tip as a profilometer during oxidation/reduction cycles driven either by consecutive potential steps or by cyclic voltammetry scans. They showed that the expulsion of cations and free solvent molecules upon oxidation implies an important shrinking of the films whereas their insertion upon reduction leads to an equally important swelling. These thickness variations appear to be reversible, independent of the potential scan rate and of the order of magnitude of the initial thickness (probably underestimated as it was measured in the dry state using SEM-FEG). More importantly, an obvious correlation between mass and thickness variations was established from the striking similarities observed between cyclic voltamassograms and cyclic voltathicknograms.

These observations open new perspectives, not only for the applications of PPy/C6S films, but also and mainly for the development of new methodologies allowing a better evaluation and understanding of ion insertion in conducting polymers and more widely in insertion electroactive materials.

References:

[1]   Z. Asfari, V. Böhmer, J. Harrofield, J. Vicens, calixarenes 2001, Kluwer Academic Publishers, Dordrecht (Netherlands), 2001.

[2]   J. Vicens, J. Harrowfield, Calixarenes in the Nanoworld, Springer, Dordrecht (Netherlands), 2007.

[3]   S. Shinkai, T. Tsubaki, T. Sone, O. Manabe, Tetrahedron Lett. 25 (1984) 5315.

[4]   S. Shinkai, K. Araki, T. Tsubaki, T. Arimura, O. Manabe, J. Chem. Soc., Perkin Trans. 1 (1987) 2297.

[5]   D.-S. Guo, K. Wang, Y. Liu, J. Inclusion Phenom. Macrocyclic Chem. 62 (2008) 1.

[6]   S. Shinkai, H. Koreishi, K. Ueda, T. Arimura, O. Manabe, J. Am. Chem. Soc. 109 (1987) 6371.

[7]   J.P. Scharff, M. Mahjoubi, R. Perrin, New J. Chem. 17 (1993) 793.

[8]   J.L. Atwood, S.J. Dalgarno, M.J. Hardie, C.L. Raston, New J. Chem. 28 (2004) 326.

[9]   L. Zhang, A. Macias, T. Lu, J. I. Gordon, G. W. Gokel, A. E. Kaifer, J. Chem. Soc., Chem. Commun. (1993) 1017.

[10]   L. Zhang, A. Macias, R. Isnin, T. Lu, G. W. Gokel, A. E. Kaifer, J. Incl. Phenom. 19 (1994) 361.

[11]   Y. Wang, J. Alvarez, A. E. Kaifer, Chem. Commun. (1998) 1457.

[12]   J. Alvarez, Y. Wang, M. Gomez-Kaifer, A. E. Kaifer, Chem. Commun. (1998) 1455.

[13]   J. M. Lehn, R. Meric, J. P. Vigneron, M. Cesario, J. Guilhem, C. Pascard, Z. Asfari, J. Vicens, Supramol. Chem. 5 (1995) 97.

[14]   Y. Zhou, C. Liu, H. Xu, H. Yu, Q. Lu, L. Wang, Spectrochim. Acta, Part A 66 (2007) 919.

[15]   C. Liu, Z. Fu, H. Yu, H. Xu, L. Wang, Y. Zhou, J. Lumin. 126 (2007) 747.

[16]   S. Kunsági-Máté, K. Szabó, B. Lemli, I. Bitter, G. Nagy , L. Kollár, Thermochim. Acta, 425 (2005) 121.

[17]   F. Perret, A.N. Lazar, A.W. Coleman, Chem. Commun. (2006) 2425.

[18]   E. Da Silva, A.N. Lazar, A.W. Coleman, J. Drug Del. Sci. Tech., 14 (2004) 3.

[19]   M. Larbony Ben-Ishay, A. Gedanken, Langmuir, 23 (2007) 5238.

[20]   M.N. Akieh, S.F. Ralf, J. Bobacka, A. Ivaska, J. Membrane Sci. 354 (2010) 162.

[21]   Z. Mousavi, J. Bobacka, A. Ivaska, Electroanalysis 17 (2005) 1609.

[22]   K. Kaneto, G. Bidan, Thin Solid Films 331 (1998) 272.

[23]   M. Vazquez, J. Bobacka, M. Luostarinen, K. Rissanen, A. Lewenstam, A. Ivaska, J. Solid State Electrochem. 9 (2005) 312.

[24]   J.M. Davey, C.O. Too, S.F. Ralph, L.A.P. Kane-Maguire, G.G. Wallace, A.C. Partridge, Macromolecules 33 (2000) 7044.

[25]   R. Nyffenegger, E. Ammann, H. Siegenthaler, R. Kötz, O. Haas, Electrochim. Acta 40 (1995) 1411.

[26]   F. Chao, M. Costa, C. Tian, Synth. Met. 75 (1995) 85.

[27]   P. Häring, R. Kötz, G. Repphun, O. Haas, H. Siegenthaler, Appl. Phys. A: Mater. Sci. Process. 66 (1998) S481.

[28]   M.F. Suárez, R.G. Compton, J. Electroanal. Chem. 462 (1999) 211.

[29]   E. Smela, N. Gadegaard, J. Phys. Chem. B, 105 (2001) 9395.

[30]   M. Skompska, A. Szkurlat, A. Kowal, M. Szklarczyk, Langmuir 19 (2003) 2318.

[31]   J.H. Hwang, M. Pyo, Synth. Met. 157 (2007) 155.

[32]   P.R. Singh, S. Mahajan, S. Rajwade, A.Q. Contractor, J. Electroanal. Chem. 625 (2009) 16.

[33]   M.J. Higgins, S.T. McGovern, G.G. Wallace, Langmuir 25 (2009) 3627.

[34]   A. Gelmi, M.J. Higgins, G.G. Wallace, Biomaterials 31 (2009) 1974.

[35]   D.A. Reece, J.M. Pringle, S.F. Ralph, G.G. Wallace, Macromolecules 38 (2005) 1616.

[36]   J. L. Atwood, D. L. Clark, R. K. Juneja, G. W. Orr, K. D. Robinson, R. L. Vincent, J. Am. Chem. Soc. 114 (1992) 7558.

[37]   J. P. Scharff, M. Mahjoubi, R. Perrin, New J. Chem. 15 (1991) 883

[38]   G. Arena, A. Contino, G. G. Lombardo, D. Sciotto, Thermochim. Acta 264 (1995) 1.

[39]   G. Diao, Y. Liu, Electroanalysis, 17 (2005) 1279.

[40]   A. Pailleret, D.W.M. Arrigan, Langmuir, 18 (2002) 9447.

[41]   A. Pailleret, N. Magan-Oliva, S. Ollivier, D.W.M. Arrigan, J. Electroanal. Chem., 508 (2001) 81.

[42]   C. Gabrielli, J.J. Garcia-Jareno, M. Keddam, H. Perrot, F. Vicente, J. Phys. Chem. B, 106 (2002) 3182.

[43]   C. Gabrielli, J.J. Garcia-Jareno, M. Keddam, H. Perrot, F. Vicente, J. Phys. Chem. B, 106 (2002) 3192.

[44]   C. Gabrielli, H. Perrot, A. Rubin, M. C. Pham, B. Piro, Electrochem. Comm., 9 (2007) 2197.

[45]   C. Gabrielli, H. Perrot, Theoretical studies of Electrogravimetry in thin Electroactive Films In Modern Aspects of Electrochemistry, Vol. 44, Ed. M. Schlesinger and R. E. White, C. G. Vayenas, p 151-238, Springer (2009).

[46]   Submitted to Electrochem. Commun.

[47]   A. Jackson, A.R. Hillman, S. Bruckenstein, I. Jureviciute, J. Electroanal. Chem., 524 (2002) 90.

[48]   J. Jacq, Electrochim. Acta, 12 (1967) 1345.

[49]   S. Bruckenstein, K. Brzezinska, A.R. Hillman, Electrochim. Acta, 45 (2000) 3801.

[50]   J. Heinze, B.A. Frontana-Uribe, S. Ludwigs, Chem. Rev., 110 (2010) 4724.

[51]   M Chourasia, G. M. Sastry, G. N. Sastry, Biochem. and Biophys. Res. Comm., 336 (2005) 961.

[52]   M.J. Ariza, T.F. Otero, J. Membrane Sci., 290 (2007) 241.
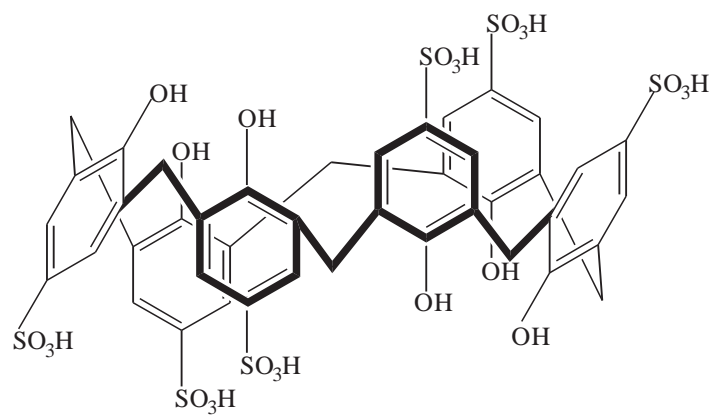
Scheme 1

Scheme 1: Molecular structure of hexasulfonated calix[6]arene (C6S)
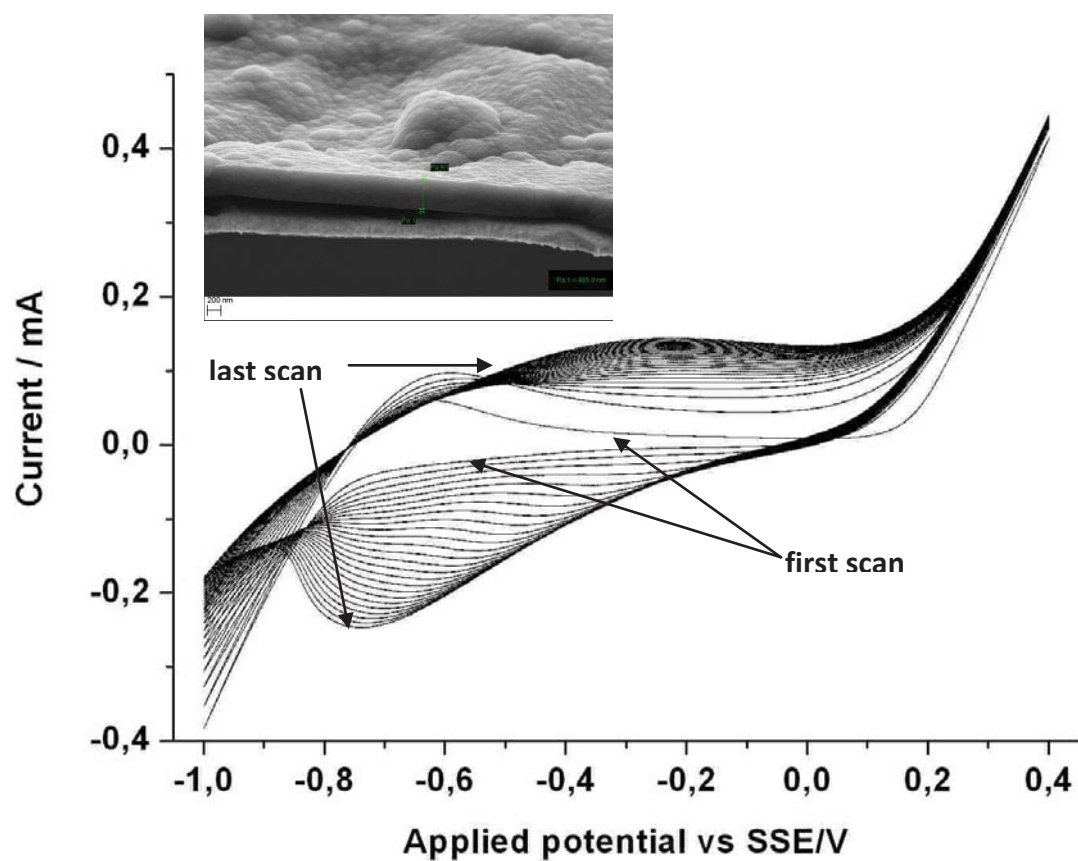
Figure 1

Figure 1 : a) typical consecutive cyclic voltammograms (25 scans) obtained during the electrodeposition of PPy/C6S from an aqueous solution containing Py (0,1 M) and C6S (1,66 mM). WE: Thin Pt layer on mica (0,126 cm^2). CE : Pt. Ref : SSE. V = 100 mV s^{-1}. b) SEM-FEG image of the profile of the resulting film.
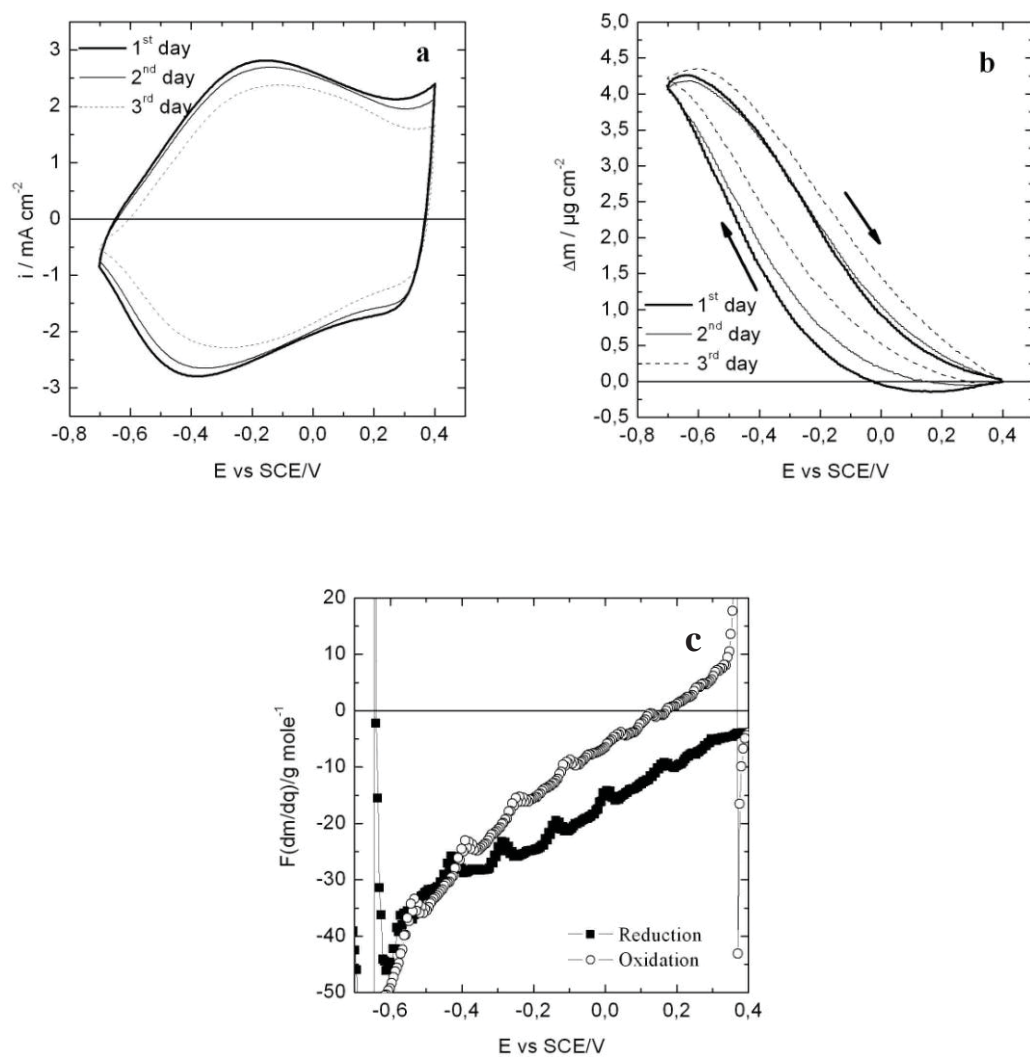
Figure 2

Figure 2 : a) typical cyclic voltammograms, b) corresponding cyclic voltamassograms obtained after transfer of the PPy/C6S film resulting from Figure 1 in a KNO_3 aqueous electrolytic solution (0,1 M) for different aging durations of the film in this solution. c) relationship between mass and charge over the whole potential range after a 16 hours aging duration. WE: golden quartz covered with a PPy/C6S film. CE : Pt. Ref : SCE. V = 100 mV s^{-1}.
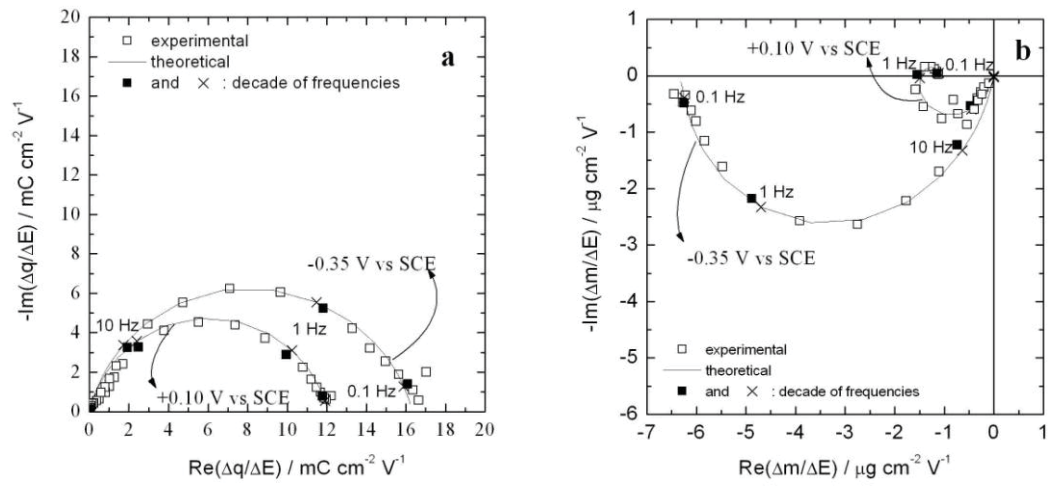
Figure 3

Figure 3: a) charge-potentiel transfer function and b) mass-potentiel transfer function at two different potentials, -0,35 V vs SCE and +0,1 V vs SCE, in 0,1 M KNO₃ aqueous solution.
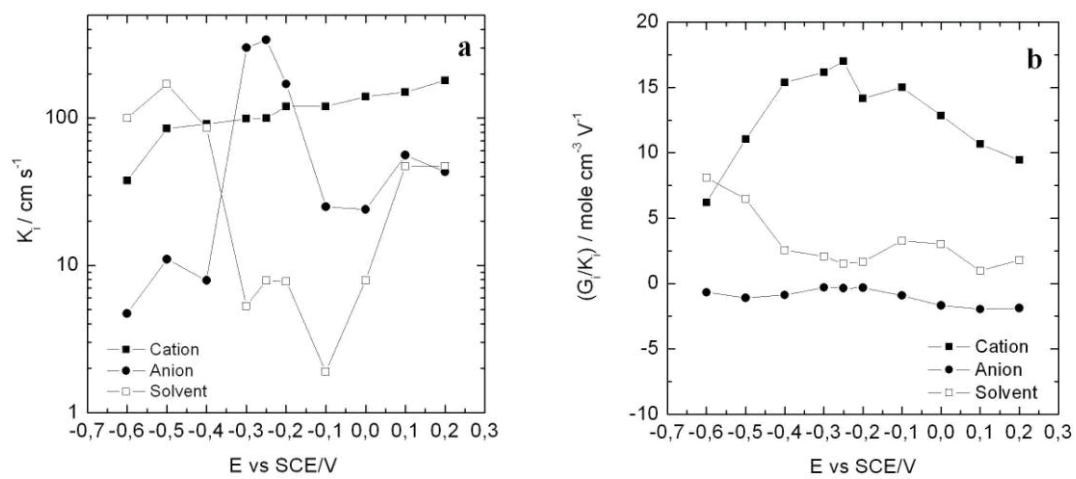
Figure 4

Figure 4: Changes of a) K_i and b) G_i / K_i ratios with respect to the potential.
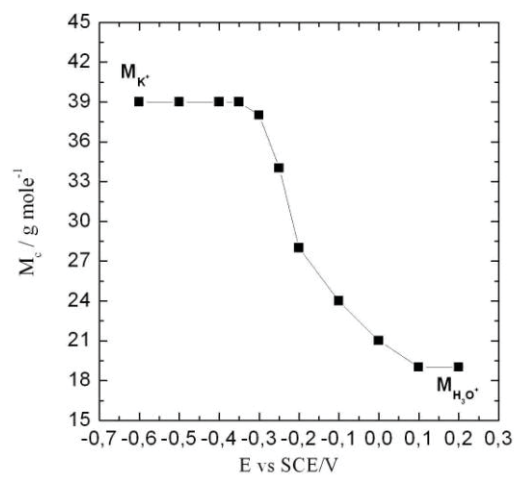
Figure 5

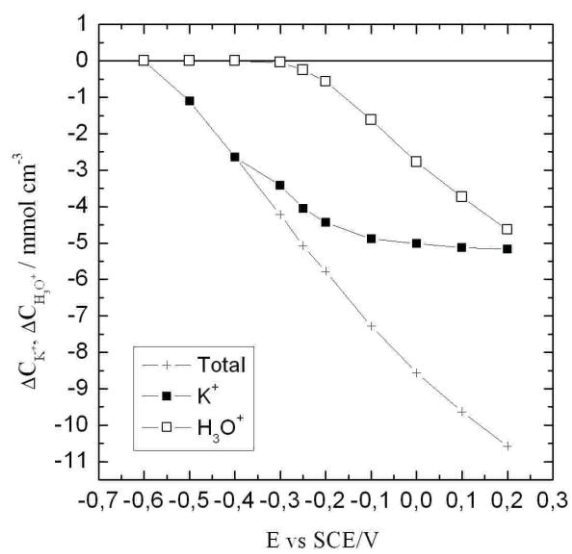Figure 5 : Apparent atomic mass of the exchanged cations

Figure 6

Figure 6: Variations of the concentrations of the expelled potassium and hydronium cations with respect to the potential.
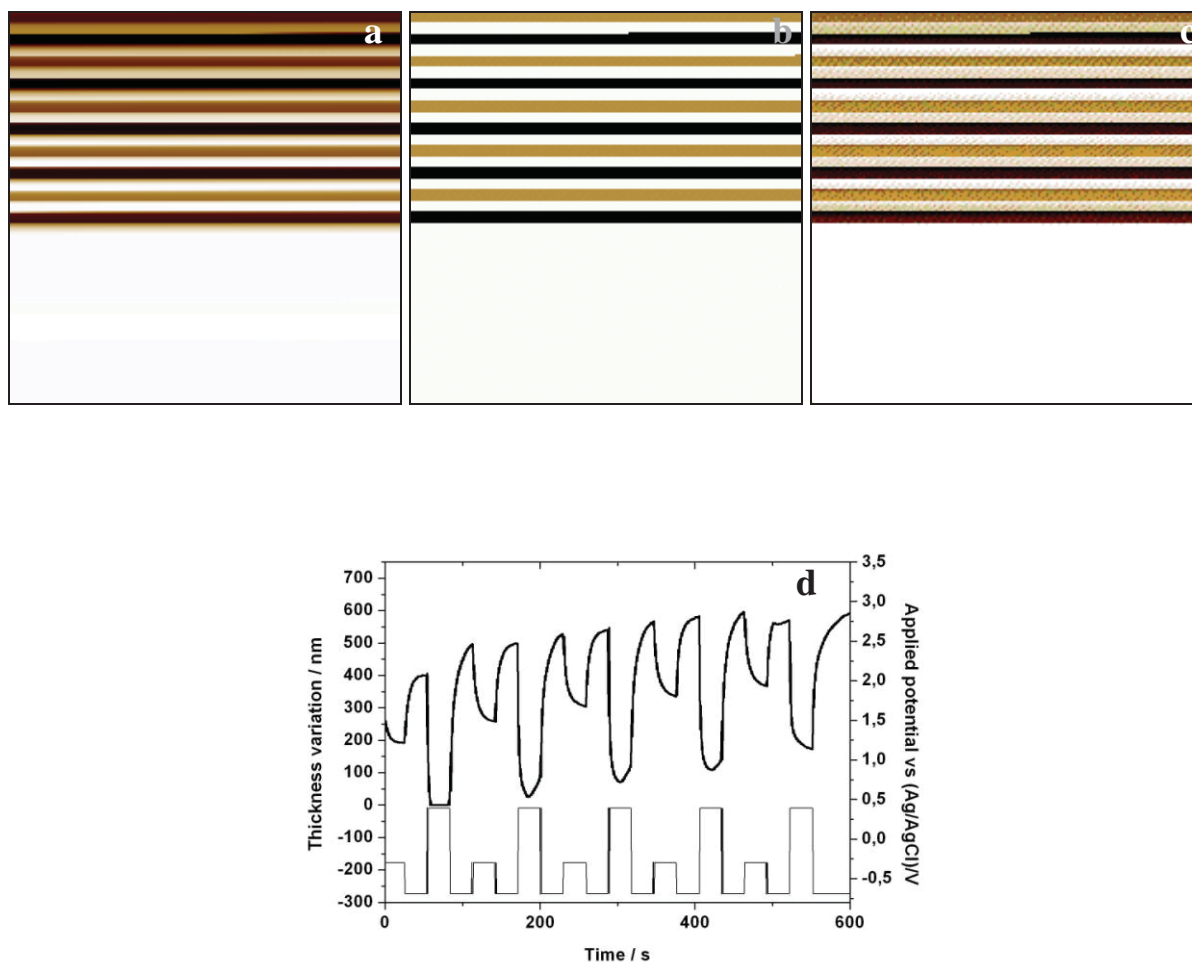
Figure 7

Figure 7 : a) Height, b) potential (with its sign inverted), and c) current images obtained by EC-AFM on a PPy/C6S film. Scan size: 1 nm^2. d) plot of height (bold line) and applied potential vs a Ag/AgCl reference electrode, extracted respectively from a) and b), as a function of time. The electrochemical conditioning is made of consecutive potential steps.
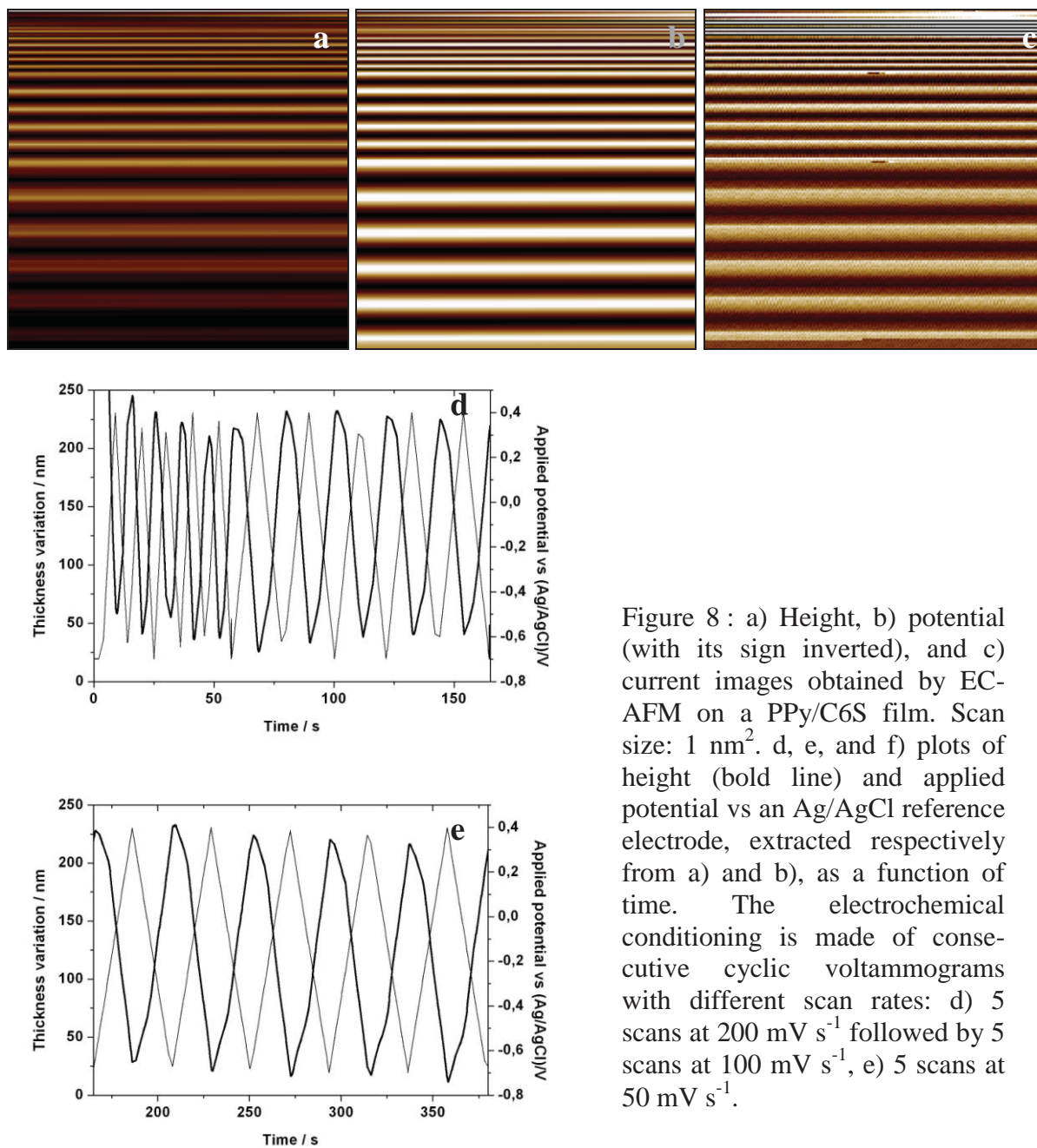
Figure 8

Figure 8 : a) Height, b) potential (with its sign inverted), and c) current images obtained by EC-AFM on a PPy/C6S film. Scan size: 1 nm^2. d, e, and f) plots of height (bold line) and applied potential vs an Ag/AgCl reference electrode, extracted respectively from a) and b), as a function of time. The electrochemical conditioning is made of consecutive cyclic voltammograms with different scan rates: d) 5 scans at 200 mV s^{-1} followed by 5 scans at 100 mV s^{-1}, e) 5 scans at 50 mV s^{-1}.
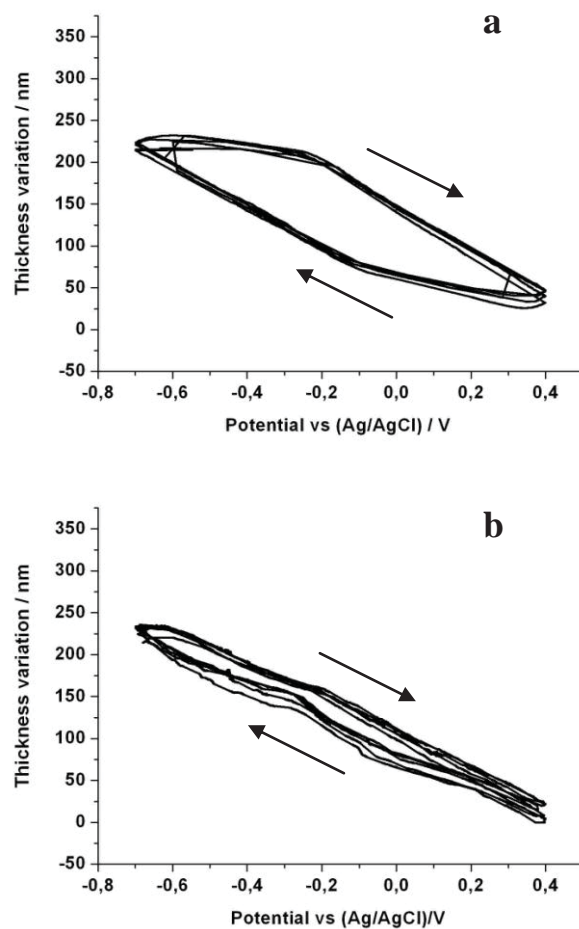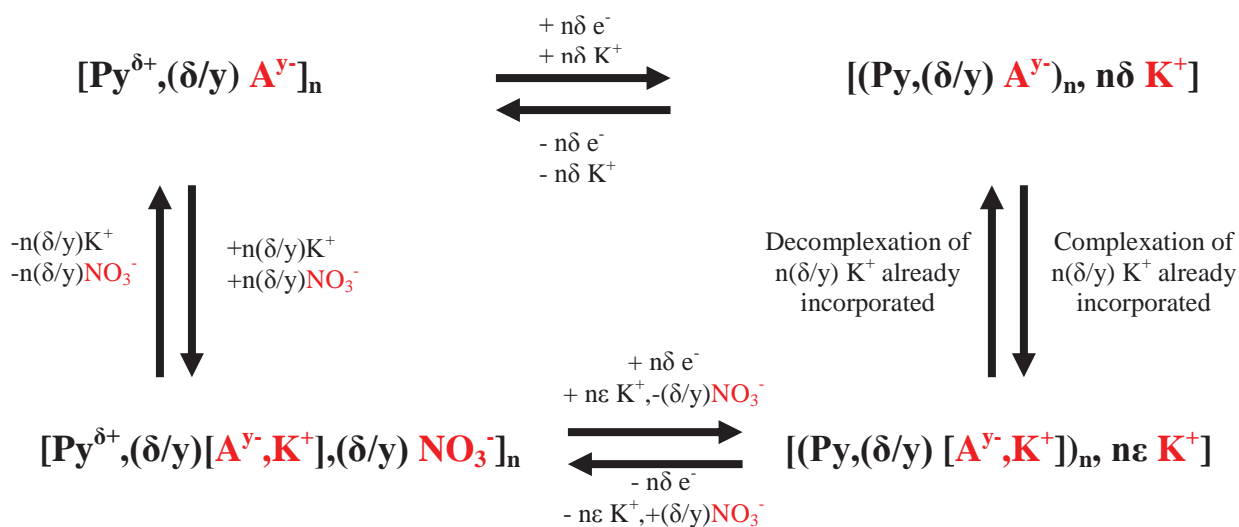
Figure 9

Figure 9 : Cyclic voltathicknogramms (5 consecutive scans) plotted from data represented on Figure 8 for a PPy/C6S film. a) 100 mV s^{-1}, b) 20 mV s^{-1}.

Scheme 2

$$+ n\delta\ e^-$$
$$+ n\delta\ K^+$$

$$- n\delta\ e^-$$
$$- n\delta\ K^+$$

$[Py^{\delta+},(\delta/y)\ A^{y-}]_n$ ⟶⟸ $[(Py,(\delta/y)\ A^{y-})_n,\ n\delta\ K^+]$

$-n(\delta/y)K^+$
$-n(\delta/y)NO_3^-$

$+n(\delta/y)K^+$
$+n(\delta/y)NO_3^-$

Decomplexation of $n(\delta/y)\ K^+$ already incorporated

Complexation of $n(\delta/y)\ K^+$ already incorporated

$$+ n\delta\ e^-$$
$$+ n\varepsilon\ K^+, -(\delta/y)NO_3^-$$

$$- n\delta\ e^-$$
$$- n\varepsilon\ K^+, +(\delta/y)NO_3^-$$

$[Py^{\delta+},(\delta/y)[A^{y-},K^+],(\delta/y)\ NO_3^-]_n$ ⟶⟸ $[(Py,(\delta/y)\ [A^{y-},K^+])_n,\ n\varepsilon\ K^+]$

Scheme 2 : Square scheme showing the behaviour of a polypyrrole film exchanging: top line) exclusively cations, bottom line) cations and anions, due to the complexation of cations in A^{y-}, whether the polypyrrole matrix is oxidised or reduced. δ: cationic charge per pyrrole unit in the oxidised polypyrrole chains ($0,25 < \delta < 0,33$), n: number of pyrrole unit in the whole film, A: C6S, y: number of anionic charges in the hexasulfonated calix[6]arene (C6S) anion irreversibly trapped in the polypyrrole matrix, $\varepsilon = \delta - (\delta/y)$.